frontiers | Frontiers in Marine Science

TYPE Original Research
PUBLISHED 17 June 2025
DOI 10.3389/fmars.2025.1538835

Impact of hydrothermal activity on marine barium isotope composition: a case study from the Southwestern Indian Ocean

Chunxiao Zhao[1], Li Li[1,2,3]*, Jiejun Li[1], Ruifang C. Xie[4,5], Xiaojing Wang[1,2] and Xuefa Shi[1,2,3]*

[1]Key Laboratory of Marine Geology and Metallogeny, First Institute of Oceanography, Ministry of Natural Resources, Qingdao, China, [2]Laboratory for Marine Geology, Qingdao Marine Science and Technology Center, Qingdao, China, [3]Shandong Key Laboratory of Deep Sea Mineral Resources Development, Qingdao, China, [4]Key Laboratory of Polar Ecosystem and Climate Change, Ministry of Education, School of Oceanography, Shanghai Jiao Tong University, Shanghai, China, [5]Shanghai Key Laboratory of Polar Life and Environment Sciences, School of Oceanography, Shanghai Jiao Tong University, Shanghai, China

The cycling of barium (Ba) is closely linked to marine biogeochemical processes. Barium and its isotopes are commonly used as tracers for marine productivity, seawater alkalinity, and ocean circulation. Mid-ocean ridge hydrothermal systems significantly impact marine chemistry, acting as key sources of trace elements in deep seawater. However, the overall contribution of hydrothermal Ba to the global Ba cycle remains poorly quantified, and studies on hydrothermal Ba isotopes are limited, hindering a comprehensive understanding of the marine Ba cycle. This study investigated the concentration of dissolved Ba and other elements, along with Ba isotope composition (δ^{138}Ba), in the hydrothermal influenced water and sediment samples collected near the Longqi and Tiancheng vents in the southwestern Indian Ocean. This constitutes the first such investigation in this region. The vertical profiles of dissolved Ba and its isotope compositions mirrored each other in the southwestern Indian Ocean, consistent with prior observations in other ocean basins. For near-field water samples, Ba isotope compositions (-0.10‰ to 0.05‰) are significantly lower than background seawater (~0.29‰). In addition, Hydrothermal sediments exhibited Ba isotopic values (-0.16‰ to 0.01‰) markedly lower than background sediments (0.01‰ to 0.14‰). The depleted δ138Ba values of near-field water samples indicate preferential removal of lighter Ba isotopes during the mixing of hydrothermal fluids with seawater. Consequently, precipitated particles acquire lighter Ba isotope signatures, explaining the low values in hydrothermal sediments. This demonstrates that sediments effectively capture and preserve hydrothermal Ba signals. Collectively, these findings provide new insights into hydrothermal influences on the marine Ba cycle.

KEYWORDS

Barium (Ba), isotope composition, hydrothermal activity, Indian Ocean, seawater, sediment

OPEN ACCESS

EDITED BY
Jessica Nicole Fitzsimmons,
Texas A and M University, United States

REVIEWED BY
Emilie Le Roy,
Woods Hole Oceanographic Institution,
United States
Wei Wei,
University of Science and Technology of
China, China

*CORRESPONDENCE
Li Li
✉ li.li@fio.org.cn
Xuefa Shi
✉ xfshi@fio.org.cn

RECEIVED 03 December 2024
ACCEPTED 26 May 2025
PUBLISHED 17 June 2025

CITATION
Zhao C, Li L, Li J, Xie RC, Wang X and Shi X (2025) Impact of hydrothermal activity on marine barium isotope composition: a case study from the Southwestern Indian Ocean. *Front. Mar. Sci.* 12:1538835.
doi: 10.3389/fmars.2025.1538835

1 Introduction

The marine barium (Ba) cycle is closely linked to marine biogeochemistry (Horner and Crockford, 2021). The primary sources of Ba in the ocean are rivers, groundwater, and hydrothermal vents (Kumagai et al., 2008; Cao et al., 2016; Carter et al., 2020; Hsieh et al., 2021). Once introduced into seawater, the dissolved Ba is removed from seawater and accumulated in marine sediments primarily in the form of the barite and in association with iron and manganese oxides (Dymond et al., 1992; Paytan and Kastner, 1996; Carter et al., 2020). The concentration of dissolved Ba in seawater is found to be associated with the concentration of the major nutrient silicon (Lea and Boyle, 1989; Jacquet et al., 2005; Roeske et al., 2012). Its sinking flux is closely linked with organic carbon flux, and it is commonly used as a tracer for marine productivity (Eagle et al., 2003; McManus et al., 1999; McCulloch et al., 2003; Paytan and Griffith, 2007). In addition, Ba displays a positive correlation with ocean alkalinity and dissolved inorganic carbon. The Ba/Ca ratio in foraminifera, for instance, can serve as a proxy for past seawater alkalinity (Lea, 1993; McManus et al., 1999).

Recently, Ba isotopes (δ^{138}Ba) have been recognized as a valuable tool for exploring the oceanic Ba cycle, providing important insights into its processes and behavior, such as, to trace the movement and mixing of deep-water masses, to serve as a proxy for marine biological productivity and to indicate riverine inputs (Horner et al., 2015; Bates et al., 2017; Hsieh and Henderson, 2017; Bridgestock et al., 2018; 2021; Crockford et al., 2019; Cao et al., 2021; Middleton et al., 2023). The Ba isotope composition in seawater ranges from 0.24‰ – 0.65‰, and the primary factor influencing the observed variations in seawater δ^{138}Ba is the formation and dissolution of barite (Horner et al., 2015; Bates et al., 2017; Hsieh and Henderson, 2017; Cao et al., 2021; Whitmore et al., 2022). Modern oceans show a significant δ^{138}Ba gradient from surface to depth, characterized by higher δ^{138}Ba values in surface water masses and lighter δ^{138} Ba values in deep water masses (Hsieh and Henderson, 2017; Bridgestock et al., 2018; Carter et al., 2020). This type of vertical distribution is a result of the precipitation process as barite from seawater, which is marked by significant isotopic fractionation, with lighter Ba isotopes preferentially incorporated into biogenic barite crystals (Horner et al., 2015; Bates et al., 2017; Hsieh and Henderson, 2017; Bridgestock et al., 2018). Similarly, adsorption onto biological particles preferentially removes lighter Ba isotopes from ambient seawater (Cao et al., 2020). Both adsorption and barite precipitation increase the δ^{138}Ba values of seawater in the upper ocean (~ 600 m), whereas the dissolution processes re-introduce lighter Ba isotopes into deeper waters.

The degree to which Ba isotopes behave conservatively in the deep ocean remains uncertain. Moreover, available published data suggest an imbalance between the sources and sinks of Ba isotopes in the modern ocean. Specifically, Ba isotope compositions from terrestrial sources range from 0.1‰ to 0.2‰, while sediment values, representing sinks, range from 0‰ to 0.1‰ (Horner and Crockford, 2021). Therefore, it is proposed that lighter Ba isotope sources or heavier isotope sinks may be missing and not fully accounted for (Horner and Crockford, 2021; Zhang et al., 2024). Bates et al. (2017) suggested that Ba isotopes exhibit conservative behavior during the mixing of North Atlantic Deep Water (NADW) and Antarctic Bottom Water (AABW) in the Atlantic. However, Hsieh and Henderson (2017) observed that in deep water between 2000 and 3000 meters, Ba isotope compositions exceeded conservative mixing predictions, reflecting additional inputs or sinks of Ba during transport, a phenomenon later explained by Hsieh et al. (2021) as resulting from hydrothermal vents imparting distinct Ba isotopic signatures to deep water masses.

Hydrothermal systems at mid-ocean ridges play a critical role in trace element recycling processes in marine system (Elderfield and Schultz, 1996; Coogan et al., 2019). Barium in source rocks is released into hydrothermal fluids through water-rock interactions under high temperatures and pressures (Von Damm, 1985), resulting in fluids highly enriched in dissolved Ba. Barium concentrations in hydrothermal fluids (1-119 μM) can be up to three orders of magnitude higher than those in seawater (30-150 nM) (Butterfield and Massoth, 1994; Kumagai et al., 2008; Seyfried et al., 2011). However, when these fluids mix with seawater, Ba precipitates as barite and is largely removed (Jamieson et al., 2016; Gartman et al., 2019). Ba also co-precipitates with metals like Fe and Cu, resulting in minimal or no net Ba flux into seawater (Carter et al., 2020). Additionally, the ultramafic lithology contrasts with the mafic-dominated settings in mid-ocean ridge vents, which may lead to unique fluid-rock interactions that modulate Ba release and isotopic fractionation (Hsieh et al., 2021; Zhang et al., 2024). To date, the research on Ba isotopes in hydrothermal systems primarily focuses on hydrothermal fluids and non-buoyant plumes, with very limited empirical data available.

To advance the understanding of the marine Ba cycle, this study investigates the geochemical characteristics and Ba isotope compositions of hydrothermal fluids, ambient seawater, and sediments from the Longqi and Tiancheng hydrothermal fields along the Southwest Indian Ridge. This research fills a gap in the study of Ba isotopes in Indian Ocean seawater and reveals the Ba isotope composition of hydrothermal end-member inputs. It is also the first investigation of Ba isotopes in hydrothermal sediments, exploring how these sediments record hydrothermal Ba inputs. The study systematically examines the mechanisms driving Ba cycling within the Southwest Indian Ridge hydrothermal system.

2 Materials and methods

2.1 Study region

The study area is located along the Southwest Indian Ridge (SWIR), an ultra-slow spreading mid-ocean ridge (Figure 1) (Demets et al., 1994; Cannat et al., 2008). The SWIR is characterized by distinctive tectonic features, including a series of large north-south trending transform faults that formed due to lateral spreading during ridge evolution. This study focuses on the Longqi and Tiancheng hydrothermal fields. The Longqi Hydrothermal Field, located at 37°47′S, 49°39′E, at a depth of

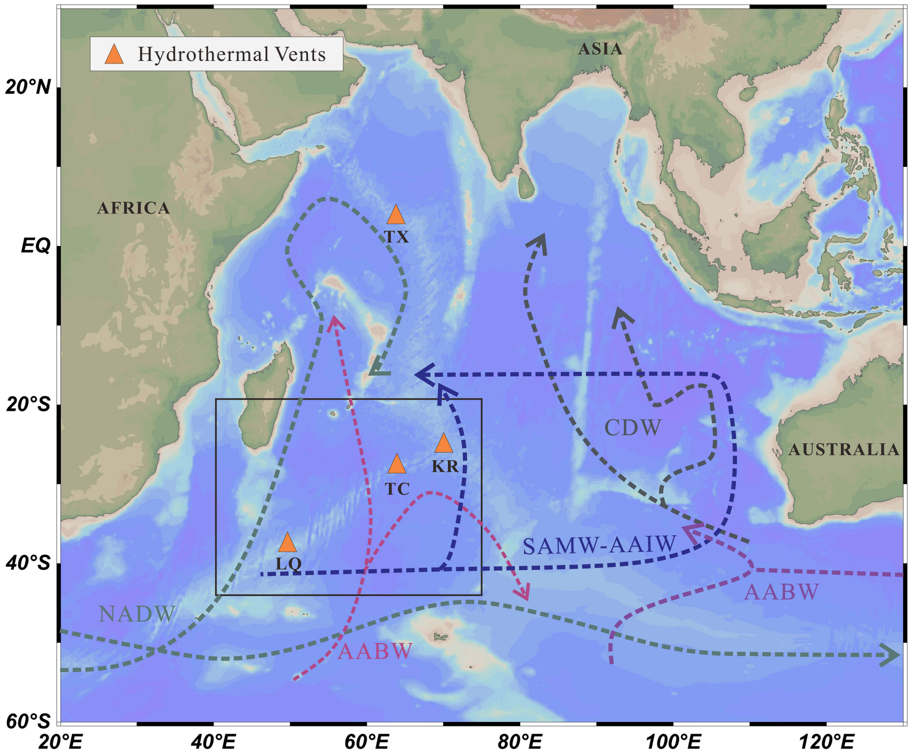

FIGURE 1
Hydrological map of india ocean the map shows the hydrothermal vent locations (orange triangles),along with the labeled main water masses SAMW (Subbantarctic Mode water) CDW (Circumpolar Deep Water AAIW) Antarctic Intermediate Water) and AABW (Antarctic Bottom Water).

2775 m, is the first active high-temperature hydrothermal field (> 300°C) discovered on the SWIR, situated on a mafic rock substrate (Tao et al., 2012). The Tiancheng Hydrothermal Field, situated at 27°51′S, 63°55′E, at a depth of 2750 meters, is the first confirmed area of low-temperature hydrothermal activity on the SWIR, with fluid temperatures around 13.2°C (Tao et al., 2014). This region experiences limited magmatic supply and intense tectonic activity, with fractured basalt as the dominant substrate (Chen et al., 2018). As shown in Figue 1, the sub-surface, intermediate, and deep layers of seawater in the study area are respectively influenced by water masses Subantarctic Mode Water (SAMW), Antarctic Intermediate Water (AAIW), Circumpolar Deep Water (CDW), and Antarctic Bottom Water (AABW) (Rippert et al., 2015; Zhang et al., 2022).

2.2 Sample collection

Water samples were collected during the DY-52 and DY-78 expeditions aboard the *R/V Da Yang 1* in April 2019 and *R/V Da Yang* in 2023, respectively. Three full-depth seawater stations (S1, S2, S3) were collected (Figure 2). Among them, S1 and S3 located directly above the Longqi and Tiancheng hydrothermal vents, respectively, and S2 represents background seawater between the two vent sites. The samples were obtained using Niskin bottles mounted on a stainless-steel rosette equipped with a CTD system (Sea-Bird® 911plus). Immediately after collection, the seawater was filtered through AcroPak capsule filters (0.2 µm, Pall Corporation®) and transferred to acid-clean low-density polyethylene (LDPE) bottles. The samples were then acidified to pH ~ 2 using high-purity nitric acid (Fisher Scientific®, Optima grade) and stored at room temperature in sealed containers. All sampling equipment, including tubes, filters, and bottles, were pre-cleaned following the protocols of Li et al. (2015).

Near-vent seawater samples (LQ-1, LQ-2, LQ-3, TC-1, TC-2, TC-3, TC-4) were collected using a custom-designed sampler mounted on the Remotely Operated Vehicle (ROV) Sea Dragon III during DY-52. The sampler was composed of a hydraulic piston, an acid-clean polycarbonate bottle, and a Teflon inlet attached to the silicone sampling tube. During DY-78, hydrothermal fluids (LQ-LT) were sampled with a titanium alloy "Pressure-Resistant Fluid Sampler" and the titanium inlet collected the fluid within the vent. Immediately after recovery of the ROV sampler, samples were filtered through polyethersulfone (PES) membranes (0.45 µm, 47 mm, Pall) and filtrate transferred to acid-cleaned LDPE bottles. They were then acidified to pH ~2 with high-purity nitric acid (Fisher Scientific®, Optima grade) and stored at room temperature. Filter membranes were preserved and stored in sealed bags for subsequent analysis.Surface sediment samples (P1–P15) were obtained from the China Ocean Sample Repository, collected during various expeditions (DY-19, 20, 21, 26, 30, 34, 35, 40, 49) using a TV grab sampler. These samples were stored in clean, sealed bags and frozen at -20°C for preservation.

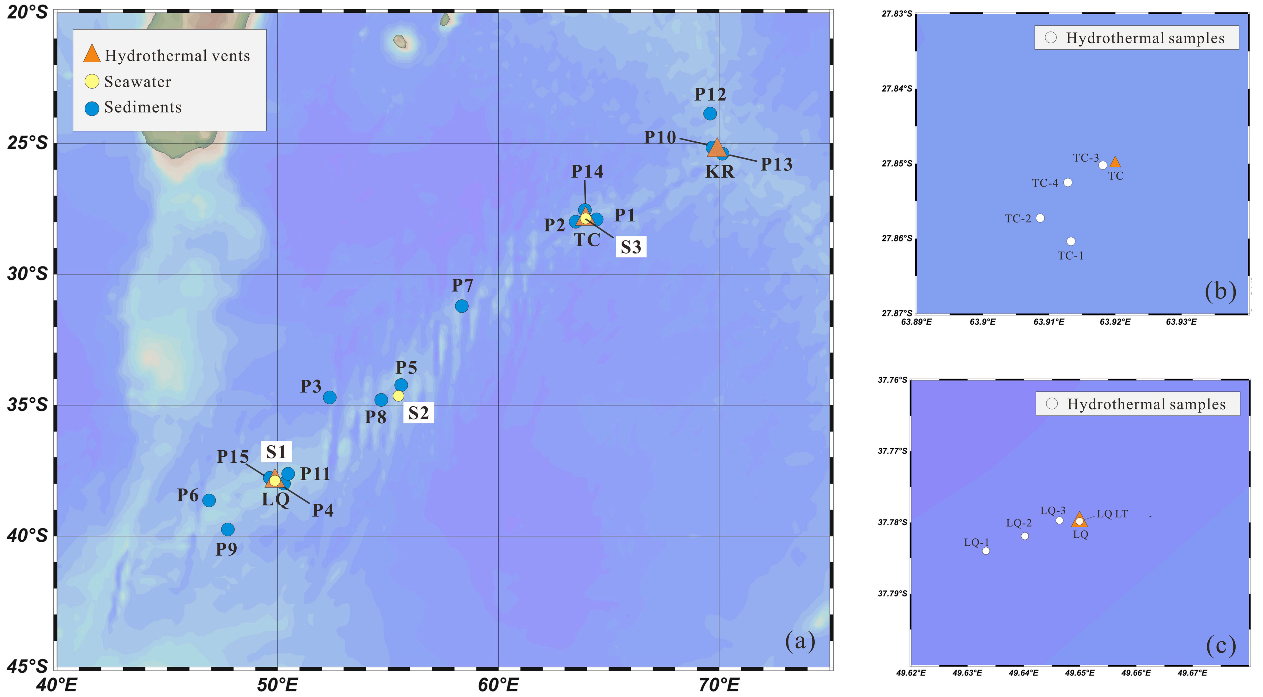

FIGURE 2
Sampling locations for seawater depth profiles hydrothermal samples and sediments Panel **(a)** presents the station locations for seawater depth profiles and sediments sampling panels **(b)** and **(c)** indicate the hydrothermal fluid and plume sampling sites at Tiancheng (TC) and longqi(LQ) .

2.3 Sample analysis

2.3.1 Analysis of seawater and hydrothermal fluid dissolved samples

Seawater and hydrothermal fluid samples were diluted 20-fold with 2% HNO_3 (Optima grade) and spiked with indium (In) as an internal standard with a final concentration of 10 ppb. Concentrations of dissolved Fe, Mnand Bawere determined using an inductively coupled plasma mass spectrometer (ICP-MS, iCAP–RQ, Thermo Fisher Scientific) in collision cell-mode at the First Institute of Oceanography of China. The precision and accuracy of Ba, Fe, Mn measurements were verified using certified reference seawater CASS-5 (National Research Council®, Canada), and the analytical results are shown in Table 1. Since no Ba data are reported in certified values of the reference seawater, the analytical results reported here are compared with data published previously by (Mori et al., 2019).

Approximately 60 ng of Ba was extracted from each stock solution and spiked with a suitable amount of the ^{130}Ba-^{135}Ba double spike. Following the methods outlined by Lin et al. (2020), the spike-sample mixtures were dried, redissolved in 2.5 mol/L HCl, and purified via column separation using AG 50 W-X8 cation-exchange resin. Procedural blanks were measured for each batch, with Ba concentrations < 0.6 ng, which was <0.1% of the total Ba in the samples. The purified samples were then dried and redissolved in 3% HNO_3 (with Ba concentrations ~ 60 ppb), and Ba isotope ratios were analyzed using a Thermo Neptune XT MC-ICP-MS at the Key Laboratory of Surficial Geochemistry, Nanjing University.

TABLE 1 Analytical results of certified reference seawater samples (CASS-5) compared to the certified values.

Parameter	Ba (nM)	Fe (ppb)	Mn (ppb)
Measured value[a]	51.84 ± 0.69(*n=4*)	1.41±0.01 (*n=3*)	2.39±0.02 (*n=3*)
Certified value	53.75[b]	1.44±0.11	0.2

[a]The data is mean ± standard deviation;
[b]Reference values are sourced from Mori et al. (2019).

Ba isotope compositions in this study are expressed as ‰ deviations (δ^{138}Ba) relative to the international Ba standard NIST SRM 3104a (Equation 1):

$$\delta^{138}\text{Ba}(\text{‰}) = \left({}^{138}\text{Ba}/{}^{134}\text{Ba}_{\text{sample}}/{}^{138}\text{Ba}/{}^{134}\text{Ba}_{\text{NIST 3104a}} - 1\right) \times 1000 \qquad (1)$$

The standard solution NIST SRM3104a and a seawater standard IAPSO were analyzed after every five samples. The Ba isotope compositions (δ^{138}Ba) of the NIST 3104a standard and IAPSO standard seawater were 0.00 ± 0.05‰ (2SD, n=11) and -0.04 ± 0.05‰, respectively. The δ^{138}Ba value for IAPSO in this study is consistent with the 0.05 ± 0.04‰ reported in a previous study (Pretet, 2013). We determined the error of the Ba isotope compositions (δ^{138}Ba) for all samples to be 0.05‰, based on the measurements of the standard SRM3104a for δ^{138}Ba (n=11).

2.3.2 Analysis of sediments

The sediment samples were freeze-dried for 48 hours and then ground into a fine powder (200-mesh). For bulk concentration analysis, approximately 50 mg of sediments (weighed to a precision of 0.1 mg) were digested in a concentrated acid mixture (HNO_3/HF, 1:1). The major elements were analyzed using inductively coupled plasma optical emission spectrometry (ICP-OES, iCAP 6300, Thermo Fisher Scientific®) with RSD < 5%, and trace elements and rare earth elements (REEs) were analyzed using ICP-MS. Sediment reference standards GBW07309 (China Reference Material) were analyzed to evaluate the reproducibility of this method (n=3). The measured values agreed well with certified values for all targeted elements (96 ± 0.6% – 105 ± 1%) and detailed information can be found in the supplementary material (Supplementary Table S1).

Approximately 100 ng of Ba was extracted from each stock digest solution for Ba isotope analysis, following the same procedure as for seawater and hydrothermal samples (Section 2.3.1). The standard solution NIST SRM3104a and a coral standard SH-1 were analyzed after every five samples. The Ba isotope compositions (δ^{138}Ba) of the coral standard SH-1 was 0.29 ± 0.04‰ (2SD, *n*=8), which was consistent with the published value of 0.31 ± 0.04‰ (Lin et al., 2022).

2.3.3 Analysis of filter membrane

The hydrothermal filter membrane was analyzed using scanning electron microscopy with energy-dispersive X-ray spectroscopy (SEM-EDX; FEI Quanta 200, Netherlands). A piece of the filter membrane (~ 0.5 cm × 0.5 cm) was attached to conductive adhesive using tweezers. The sample was then coated with gold for 25 seconds under vacuum conditions, after which it was placed under the scanning electron microscope for observation, with the aim of identifying as many different types of mineral particles as possible.

3 Result and discussion

3.1 Dissolved Ba concentrations and its isotope compositions of seawater

3.1.1 Characteristics of barium concentrations and isotopic distributions in this study

Vertical distribution of dissolved Ba concentrations ($[Ba]_{diss}$) at stations S1, S2 and S3 are shown in Figure 3 and Table 2. The dissolved Ba concentrations range from approximately 37 to 107 nM, with a typical increasing pattern from surface to bottom. The concentration varied slightly within the surface 1000 m (37 – 50 nM), and increased sharply to over 80 nM at 2000 m. S3, the station located above the Tiancheng hydrothermal vent, had a higher $[Ba]_{diss}$ (~ 90 nM) compared to the ones further south (S1 and S2). Barium is considered a bio-intermediate element, with its dissolved concentrations ($[Ba]_{diss}$) in the water column typically following a nutrient-like depth profile. In surface waters, $[Ba]_{diss}$ is reduced due to its removal via association with marine particles. However, $[Ba]_{diss}$ becomes enriched in deep water, primarily as a result of the decomposition and remineralization of settling particles (Lea and

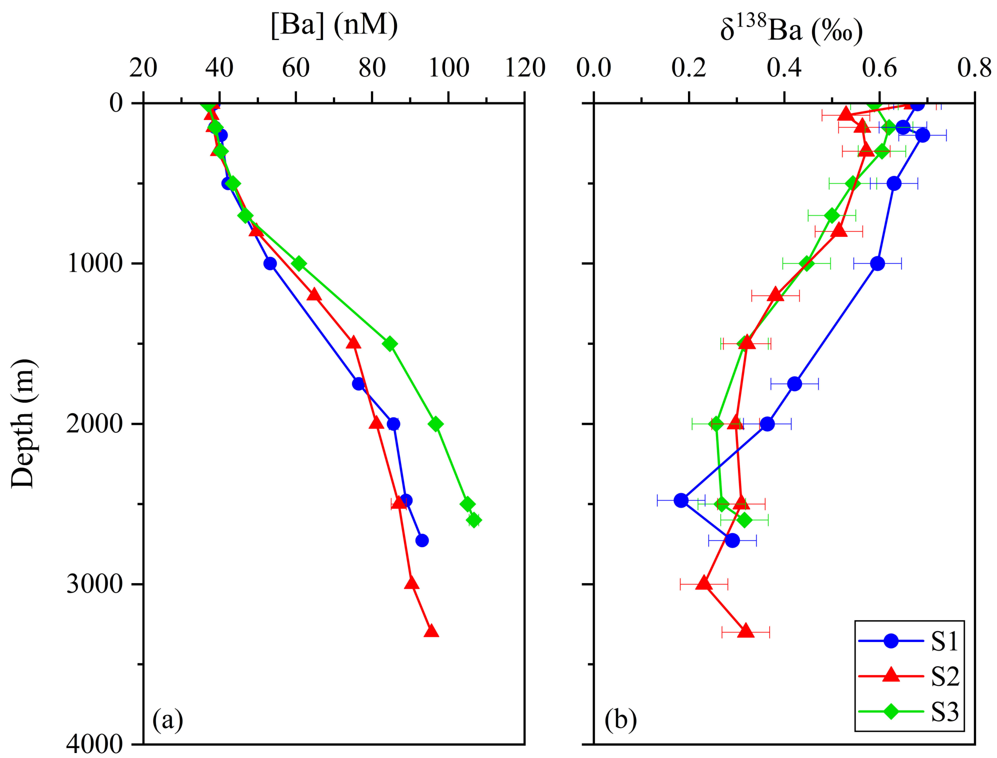

FIGURE 3
Depth profiles of seawater showings **(a)** dissolved Ba concentrations and **(b)**.

TABLE 2 The concentrations of Ba and Ba isotope compositions in seawater samples.

Station	Depth(m)	Ba(nM)	δ^{138}Ba
S1	3	38.49	0.68
	150	38.78	0.65
	200	40.37	0.69
	500	42.26	0.63
	1000	53.27	0.60
	1750	76.52	0.42
	2000	85.65	0.36
	2477	88.89	0.18
	2727	93.14	0.29
S2	5	38.13	0.67
	75	37.91	0.53
	150	38.38	0.56
	300	39.58	0.57
	800	49.68	0.51
	1200	64.87	0.38
	1500	75.17	0.32
	2000	81.18	0.30
	2500	86.98	0.31
	3000	90.42	0.23
	3300	95.60	0.32
S3	5	36.93	0.59
	50	38.30	no data
	150	38.96	0.62
	300	40.31	0.61
	500	43.52	0.54
	700	46.76	0.50
	1000	60.80	0.45
	1500	84.70	0.32
	2000	96.74	0.26
	2500	105.10	0.27
	2600	106.74	0.32

Boyle, 1991; Hsieh and Henderson, 2017; Carter et al., 2020; Yu et al., 2022).

In contrast, δ^{138}Ba values decrease from 0.65‰ near the surface to about 0.20‰ at greater depths (Figure 3). This inverse relationship between Ba concentration and isotope composition mirrors the vertical distributions that have also been observed in the Atlantic and Pacific Oceans (Figure 4) (Horner et al., 2015; Hsieh and Henderson, 2017). The observed profiles are attributed to isotopic fractionation that occurs during pelagic barite precipitation while its dissolution process shows negligible isotopic fractionation. Different from $[Ba]_{diss}$ in which all three water profiles shown similar trends and values with depth, the vertical profiles of δ^{138}Ba for stations S2 and S3 are quite similar, and δ^{138}Ba for stations S1 and S2 are also exactly similar (S1: 0.68‰;S2: 0.67‰) while the ones for S1 are heavier by ~ 0.1——0.2 ‰ within the top 2000 m. At 2500 m, the δ^{138}Ba at S1 (0.18 ± 0.05‰) is marginally lower than at S2 (0.31± 0.05‰) and S3 (0.27 ± 0.05‰), though the difference is within analytical uncertainty (Figure 3). The relationship between dissolved Ba concentrations and Ba isotope compositions (δ^{138}Ba) is displayed in Supplementary Figure S1, revealing a statistically significant negative correlation ($p < 0.01$). In addition, the temperature and salinity of the seawater samples are plotted in the T-S diagram (Figure 5). With the exception of a few surface seawater samples, all data points form distinct curves or clusters, and no extreme temperature or salinity characteristics are observed. These results indicate that the analyzed seawater samples do not exhibit significant influence from hydrothermal input.

3.1.2 Comparison with global barium cycling trends

The comparison of the vertical profile of station S2 with the ones in other ocean basins is shown in Figure 4. Except for the vertical distribution in the Southern Ocean, $[Ba]_{diss}$ in S2 in this study always lie between those from the Pacific Ocean and Atlantic Ocean, both in surface waters and deep waters. In surface waters, the $[Ba]_{diss}$ are relatively higher (~ 45 nM) in the Atlantic Ocean and lower (~ 30 nM) in the Pacific Ocean, while the opposite is true in deep waters. The $[Ba]_{diss}$ in deep waters are relatively higher (~130 nM) in the Pacific Ocean and lower in the Atlantic Ocean (~ 70 nM), with the ones found in this study similar to the deep water in the Southern Ocean (~ 90 nM).

While the study by Jacquet et al. (2005) on barium in the Crozet–Kerguelen Basin demonstrated that barite precipitation can induce surface water alterations in the Southern Ocean, recent investigations of dissolved Ba concentrations in water column profiles from the high-latitude Southern Ocean (Weddell Sea) have revealed that the Southern Ocean exhibits relatively high $[Ba]_{diss}$ in surface waters, with minimal variation between surface and deep waters (Yu et al., 2022). This limited variation is attributed, in part, to the region's classification as a high nutrient, low chlorophyll (HNLC) zone, where restricted barite formation leads to minor changes in surface water $[Ba]_{diss}$ (Fu and Wang, 2022; Yu et al., 2022). Additionally, the strong upwelling of Circumpolar Deep Water (CDW) from below further reduces the extent of $[Ba]_{diss}$ variation throughout the water column (Hsieh and Henderson, 2017; Yu et al., 2022).

Overall, deep-water $[Ba]_{diss}$ follows the sequence: North Pacific > South Pacific > Southern Ocean > Southwest Indian Ocean > South Atlantic > North Atlantic. This trend correlates positively with the age of the water masses, i.e., the older the water mass, the higher the $[Ba]_{diss}$, which again is the accumulation result of the dissolution of barite in deep water.

The comparison of the δ^{138}Ba values of the vertical profile of station S2 with the ones in other ocean basins is shown in Figure 4. Similar to the distribution of $[Ba]_{diss,}$ the δ^{138}Ba found in S2 in this study is between those in the Pacific and Atlantic Oceans in deep waters. The δ^{138}Ba values in deep waters are relatively higher (~ 0.45‰) in Atlantic Oceans and lower in Pacific Oceans (~ 0.25‰), and the ones found in this study is ~ 0.30‰. Likewise, The Southern Ocean exhibits relatively light Ba isotope compositions in deep water, with minimal variation between surface and deep waters. The δ^{138}Ba values show an inverse relationship to water mass age, indicating that lighter Ba isotopes are released into seawater during barite particle dissolution.

3.2 Geochemical processes near hydrothermal vents

3.2.1 Dissolved Mg, Fe and Mn distributions

Deep-sea hydrothermal vent fluids are in a reduced state and highly enriched in dissolved trace metals such as Fe, Mn, Cu, and Zn, with concentrations several orders of magnitude higher than those in surrounding seawater (Rouxel et al., 2008; Findlay et al., 2019; Gartman et al., 2019). When these high-temperature, reducing hydrothermal fluids mix with cooler, oxygenated seawater, most trace metals precipitate as sulfides or oxides near the vent (Rouxel et al., 2016; Yuan et al., 2018). Recently, GEOTRACES studies have shown that a portion of these metals (Fe, Zn, Cu) released from the hydrothermal vents can be stabilized as organic complexes or nanoparticles, remaining in the dissolved phase, and transported over thousands of miles (Bennett et al., 2009; Hawkes et al., 2013; Li et al., 2014; Fitzsimmons et al., 2017; Lough et al., 2019).

Dissolved Mg, Fe, Mn, Ba concentrations and Ba isotope compositions in samples collected in and near the hydrothermal vents in this study are reported in Table 3. Dissolved Mg concentrations are commonly used to indicate the extent of seawater mixing with hydrothermal fluids. During hydrothermal fluid-rock interactions, Mg is typically removed as magnesium silicates, so that Mg concentration in hydrothermal fluids that is not mixed with seawater (termed unmixed hydrothermal fluids hereafter) should approach zero theoretically (Alt, 1995; Mottl et al., 1978). This inference is supported by Ji et al. (2017) who reported that Mg concentration in unmixed hydrothermal fluids from the Longqi hydrothermal field is 1.41 mM. Conversely, the background seawater adjacent to Longqi hydrothermal vent has a concentration of Mg of 52.5 mM (Gallant and Von Damm, 2006), significantly higher than that in unmixed hydrothermal fluids.

In this study, the Mg concentrations were found to range from 40.9 to 54.2 mM. One sample, referred to as "hydrothermal fluid" (LQ-LT), collected within the vent during the DY-78 expedition, had a Mg concentration of 40.9 mM, suggesting that mixing with background seawater had already occurred within the vent. In addition, the plume samples (LQ-1, LQ-2, LQ-3, TC-1, TC-2, TC-3, TC-4), collected near hydrothermal vents, exhibited Mg concentrations between 51.8 and 54.2 mM, indicating that these samples were highly mixed with seawater.

Despite the high degrees of mixing with background seawater, dissolved Fe and Mn concentrations in these samples were significantly higher than those reported in background seawater (Fang and Wang, 2021), indicating a notable contribution from hydrothermal sources. The relationship between Fe and Mn concentrations and their distance from hydrothermal vents is shown in Figure 6. The results reveal that among the hydrothermal samples from the Longqi vent, the fluid sample LQ-LT collected from

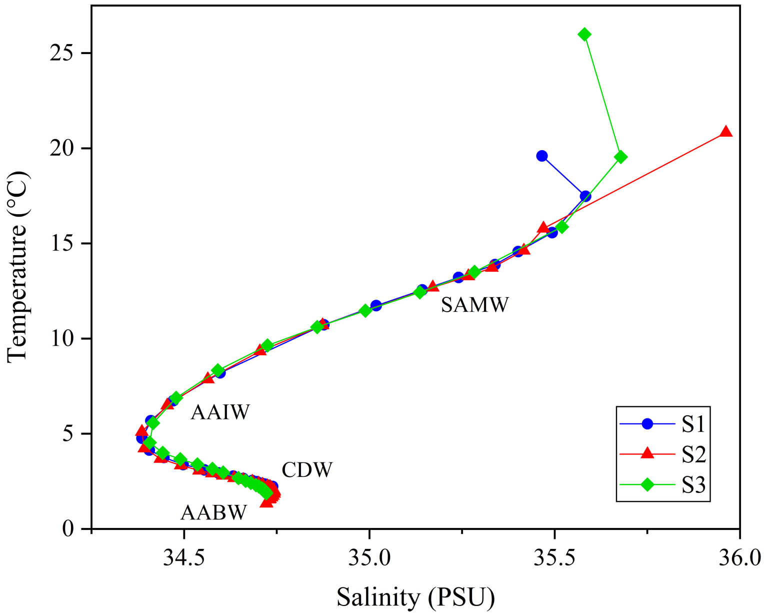

FIGURE 4
Temperature-Salinity(T-S) diagram of seawater.

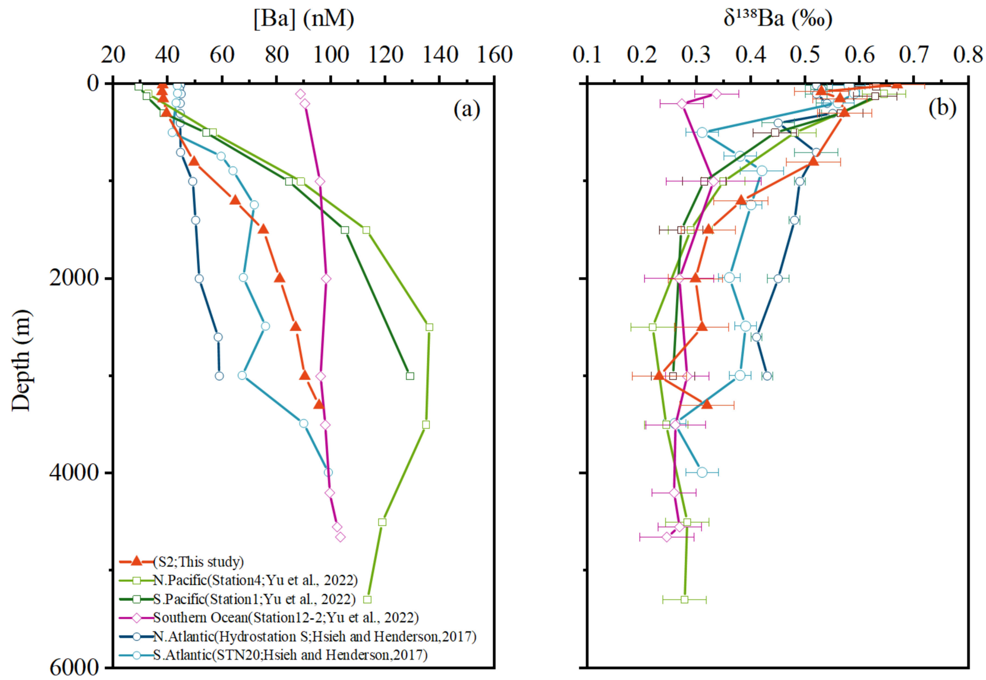

FIGURE 5
Depth profiles of **(a)** dissolved Ba concentrations and **(b)** Ba isotope compositions Data for the North pacific south Pacific and souththern Ocean are from Yu et al (2022) while data for the North atlantic and South atlantic are from Hsieh and Henderson (2017).

the vent interior exhibits the highest dissolved Fe and Mn concentrations, with concentrations rapidly declining in the remaining plume samples. All hydrothermal samples from the Tiancheng vent belong to plume samples, showing significantly lower Fe and Mn concentrations compared to the fluid sample (LQ-LT). Furthermore, Fe and Mn data from both vents indicate that only two samples (LQ-LT and TC-3) collected in close proximity to the hydrothermal vents display higher Fe concentrations than Mn concentrations. In all other plume samples, Mn concentrations decline at a slower rate relative to Fe. Previous studies have reported that during the mixing of hydrothermal fluids and seawater, dissolved Mn tends to be more stabilized in dissolved phase compared to Fe, the latter of which is removed as particles quite quickly during this process (Resing et al., 2015; Fitzsimmons et al., 2017). The distribution characteristics of these metals provide critical fluid mixing context for understanding barium isotope fractionation in hydrothermal systems.

3.2.2 The dissolved Ba distributions and Ba isotope composition

The hydrothermal samples exhibited dissolved barium concentrations ($[Ba]_{diss}$) ranging from 93 to 869 nM (Figure 6). Notably, two samples showed exceptionally high values: the hydrothermal fluid LQ-LT (869 nM) and the plume sample TC-3

TABLE 3 The concentrations of Fe, Mn, Mg, Ba, Ba isotope compositions and distance from vents in hydrothermal samples.

Sample ID	Sample type	Distance (km)	Fe (nm)	Mn (nM)	Mg (mM)	$[Ba]_{diss}$ (nM)	δ^{138}Ba (%)
LQ-LT	fluid	0	310 μM	130 μM	40.9	869	-0.01
LQ-1	plume	1.56	8.84	107	52.5	93	0.27
LQ-2	plume	0.86	153	1.31 μM	53.4	97	0.26
LQ-3	plume	0.26	395	684	52.3	102	0.20
TC-1	plume	1.40	68.0	439	54.2	113	0.22
TC-2	plume	1.48	37.8	374	52.8	126	0.23
TC-3	plume	0.20	1.81 μM	930	51.8	738	-0.10
TC-4	plume	0.82	72.8	1.65 μM	54.0	198	0.05
Background seawater			0.54-1.07^c	0.18-0.24^c	52.5 ^{c}	89^d	0.29 ^{d}

^{c}The concentration values of Fe, Mn, and Mg were referenced from previous published data (Nishioka et al., 2013; Schlitzer et al., 2018; Gallant and Von Damm, 2006).
^{d}The [Ba]diss and δ^{138}Ba data of background seawater were calculated as averages based on data measured in this study at station S2 from samples collected at depth of 2000 meters and below.

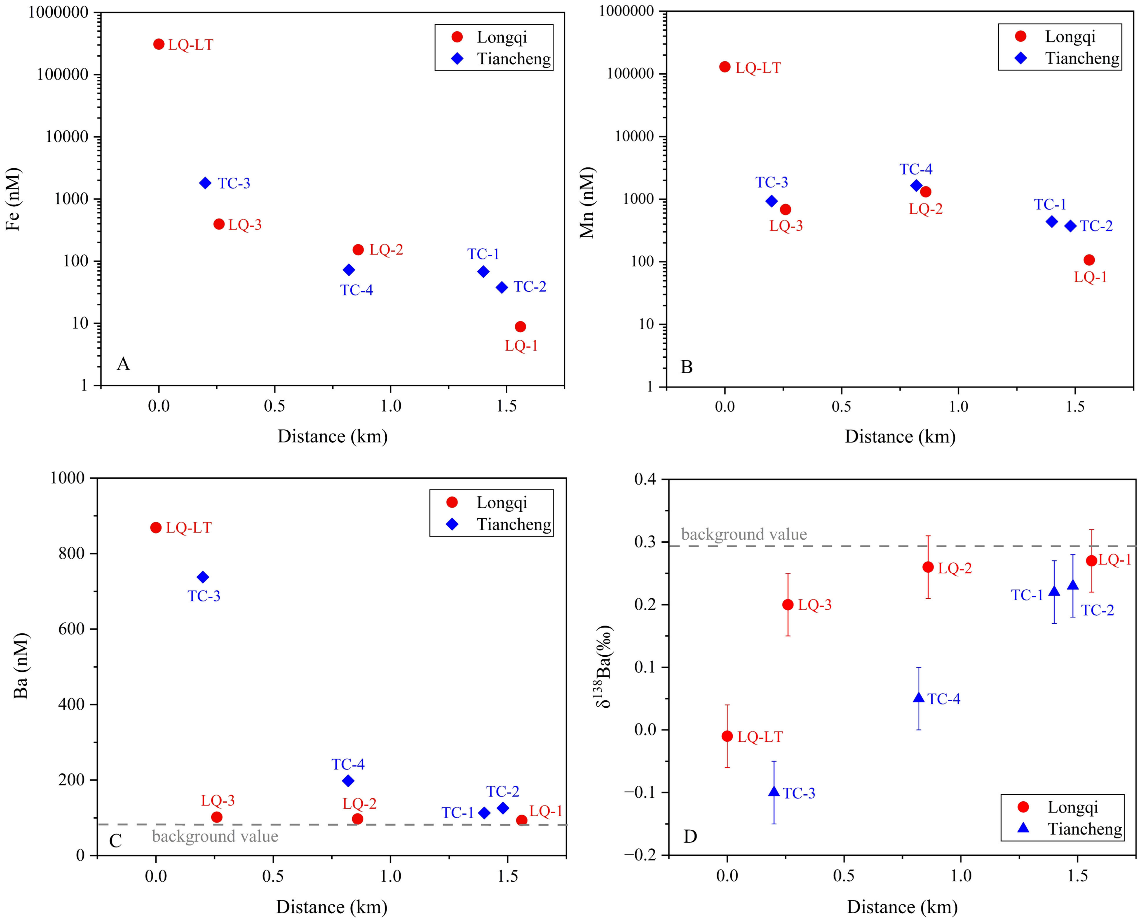

FIGURE 6
Fe, Mn, Ba concentrations and δ^{138}Ba with distance from the Tiancheng (TC) and Longqi (LQ) hydrothermal vents.

(738 nM). Excluding these, the remaining of plume samples displayed a narrower concentration range (93-198 nM). Given the limited reported [Ba]diss data for the Indian Ocean, we calculated a background seawater value (~89 nM) by averaging measurements from station S2 (located away from hydrothermal vents) at depths≥2000 m. All hydrothermal samples exceeded this background value, demonstrating a clear influence of hydrothermal input on Ba enrichment.

The δ^{138}Ba in hydrothermal samples ranged from -0.10 to 0.27‰ and it exhibits a positive correlation with the distance from the hydrothermal vent (Figure 6). The two samples with the nearest distance and highest $[Ba]_{diss}$, LQ-LT and TC-3, had lightest isotope composition -0.01‰ and -0.10‰, respectively, significantly lower than δ^{138}Ba values found in background seawater (0.29 ‰) in this study. The station with the third highest Ba concentration, TC-4, also had a light Ba isotope composition, being 0.05‰. The Ba isotopic compositions (δ^{138}Ba) of samples from the Tiancheng (TC) hydrothermal vent exhibit relatively lower values compared to those from the Longqi (LQ) vent, albeit within analytical uncertainty. Furthermore, the δ^{138}Ba values of TC samples display a slower rate of change with increasing distance from the vent, whereas LQ samples show a rapid increase in δ^{138}Ba values as distance from the vent increases. This contrast likely reflects differences in Ba isotope behavior under distinct geological settings. The Longqi Hydrothermal Field is an active high-temperature system (>300°C) hosted in mafic rocks (Tao et al., 2012). In contrast, the Tiancheng Hydrothermal Field is characterized by low-temperature hydrothermal activity (fluid temperatures ≈13.2°C; Tao et al., 2014), limited magmatic supply, and intense tectonic activity, with fractured basalt dominating the substrate (Chen et al., 2018). These geological disparities—specifically, variations in thermal regimes, host rock composition, and tectonic stress—may govern the observed differences in Ba isotope fractionation and transport dynamics between the two vent fields. Overall, the hydrothermal samples closer to the vents with high $[Ba]_{diss}$ (LQ-LT, TC-3, TC-4) have a mean δ^{138}Ba value of -0.02‰(SD=0.07‰), significantly lower than that of background seawater (0.29‰, SD=0.04‰), which suggests that the hydrothermal vent introduce lighter Ba into surrounding seawater. The Ba isotope compositions of hydrothermal fluids from the Longqi vent field (δ^{138}Ba = −0.01‰) and plume samples near the Tiancheng vent field (δ^{138}Ba = −0.10‰ to +0.05‰) on the Southwest Indian Ridge (SWIR) align closely with the range of initial endmember vent fluids (−0.17‰ to +0.09‰) reported by Hsieh et al. (2021) for mid-ocean ridge (MOR) systems. This consistency suggests that the Ba isotopic signatures of the SWIR fluids are primarily controlled by water-rock interactions with oceanic crustal lithologies, similar to other MOR hydrothermal systems. The Longqi fluid value (−0.01‰) approaches the range of mid-ocean ridge basalts (MORBs: +0.02‰ to +0.15‰; Nielsen et al., 2018) and falls within the range of pelagic sediments (−0.21‰ to +0.11‰; Bridgestock et al., 2018), supporting Hsieh et al.'s conclusion that Ba isotopes are not significantly fractionated during high-temperature fluid-rock reactions. Notably, the SWIR data lack the extremely heavy δ^{138}Ba values (up to +0.91‰) observed in sediment-influenced systems like the Main Endeavour Field (MEF) (Hsieh et al., 2021). This absence reinforces Hsieh et al.'s finding that sediment interaction can elevate fluid Ba isotope ratios, a process unlikely in the ultramafic- or basalt-hosted SWIR vents. Instead, the SWIR results align more closely with basalt-dominated systems (e.g., East Pacific Rise), further emphasizing the role of host rock composition in shaping initial fluid signatures. These comparisons highlight the utility of Ba isotopes in tracing hydrothermal contributions to oceanic Ba cycling, while underscoring the need to account for local geological and physicochemical conditions when interpreting isotopic variability.

3.2.3 Ba isotopic fractionation during hydrothermal fluids-seawater mixing

Previous studies on Ba isotopes in hydrothermal systems remain limited (Hsieh et al., 2021; Zhang et al., 2024). Hsieh et al. (2021) examined Ba isotopes in hydrothermal fluids and particulates from multiple vents. After correcting for particulate data, they reported Ba isotope compositions in endmember hydrothermal fluids ranging from -0.17‰ to 0.09‰, which are lighter than background seawater. They calculated an isotope fractionation factor ($\Delta^{138}/^{134}\text{Ba}_{\text{Dregs-fluid}}$) of -0.35‰ during the mixing of hydrothermal fluids with seawater, suggesting preferential removal of lighter Ba isotopes. Modeling with this fractionation value, they further inferred that the Ba isotope composition would increase to +1.7 ± 0.7‰ when barite becomes undersaturated, indicating a potential contribution of heavier Ba isotopes from hydrothermal systems to the ocean. In contrast, Zhang et al. (2024) performed direct measurements on non-buoyant plume samples from the Rainbow hydrothermal field and found the δ^{138}Ba values of hydrothermally affected deep seawater exhibit a lighter isotopic signature (~ 0.3‰) compared to those found at similar depths at distant locations in the Atlantic Ocean (~ 0.45‰). Interestingly, they found that dissolved Ba undergoes conservative mixing between Rainbow hydrothermal endmember fluids and the non-buoyant plume, as evidenced by a significant linear correlation between dBa and ^{3}He. However, the Rainbow is an ultramafic system, distinct from most mafic-hosted vents. The linear regression used for Rainbow is based on a single sample and whether the conservative Ba behavior observed in the Rainbow field also occurs in other hydrothermal systems is unknown. To better constrain the global hydrothermal Ba inputs, more observations in hydrothermal plumes are required.

In this study, we also found the hydrothermal fluid and plume samples with high concentration of Ba exhibited lighter Ba isotope compositions, ranged from -0.10‰ to 0.05 ‰, which is consistent with the result reported in the previous study (Zhang et al., 2024). The relationship between dissolved Ba concentrations and Ba isotope compositions (δ^{138}Ba) is displayed in Supplementary Figure S2. One station in our samples (TC-4) exhibited a dissolved Ba concentration of 198 nM, closely matching the effective input Ba concentration of 200 nM calculated in Hsieh et al. (2021). However, the Ba isotope composition at TC-4 was 0.05‰, substantially lighter than the model-based value (+1.7 ± 0.7‰) reported by Hsieh et al. (2021). This significant discrepancy between the observed isotopic composition and the model-predicted endmember values raises a critical question: what mechanisms drive the marked deviation, particularly given the opposing trends?

It is critical to consider that Ba may be sequestered from hydrothermal fluids via coprecipitation with iron-manganese oxides and sulfide minerals, as well as adsorption onto authigenic particulates, processes that can significantly influence its isotopic fractionation (Rouxel et al., 2016; Yuan et al., 2018). Previous studies indicate that in high-temperature hydrothermal environments, anhydrite has a higher saturation index than barite, which suggests that anhydrite may precipitate firstly, thereby limiting barite precipitation (Jamieson et al., 2016). Zhang et al. (2024) also highlighted the complexity of barite precipitation and Ba removal in hydrothermal systems. Therefore, assuming the Ba removal is solely due to barite formation, as proposed by Hsieh et al. (2021), may not be correct. As reported by previous studies, trace elements are often precipitated with particles released from hydrothermal vents (Rouxel et al., 2016; Yuan et al., 2018). Analysis of filter membranes from Longqi and Tiancheng hydrothermal vents samples using Scanning Electron Microscopy and Energy-Dispersive X-ray Spectroscopy (SEM-EDX; FEI Quanta 200) revealed that, various mineral species exist in addition to barite, such as Fe oxides, FeS, FeS_2, $Fe_{(1-x)}$ Sx, CeO_2, ZnS, and SiO_2, etc. (Figures 7A; 7B). Therefore, barium may co-precipitate with iron-manganese oxides and metal sulfide particles in addition to forming barite; these various processes could result in different isotopic fractionation. Further studies should be conducted to investigate the Ba isotopic fractionation associated with different removal processes.

3.3 Sediments near hydrothermal field

3.3.1 Geochemical characteristics

As discussed in the previous section, some elements (e.g. Fe, Mn, Cu, Zn) enriched in hydrothermal fluids typically precipitate with particles, and eventually settle to the seafloor near the vents (Liao et al., 2018). Even after alteration during early diagenesis processes, the hydrothermal elements that are enriched in sediments in general remain stable (Feely et al., 1987; Li et al., 2015; Agarwal et al., 2020). These sediments preserve geochemical

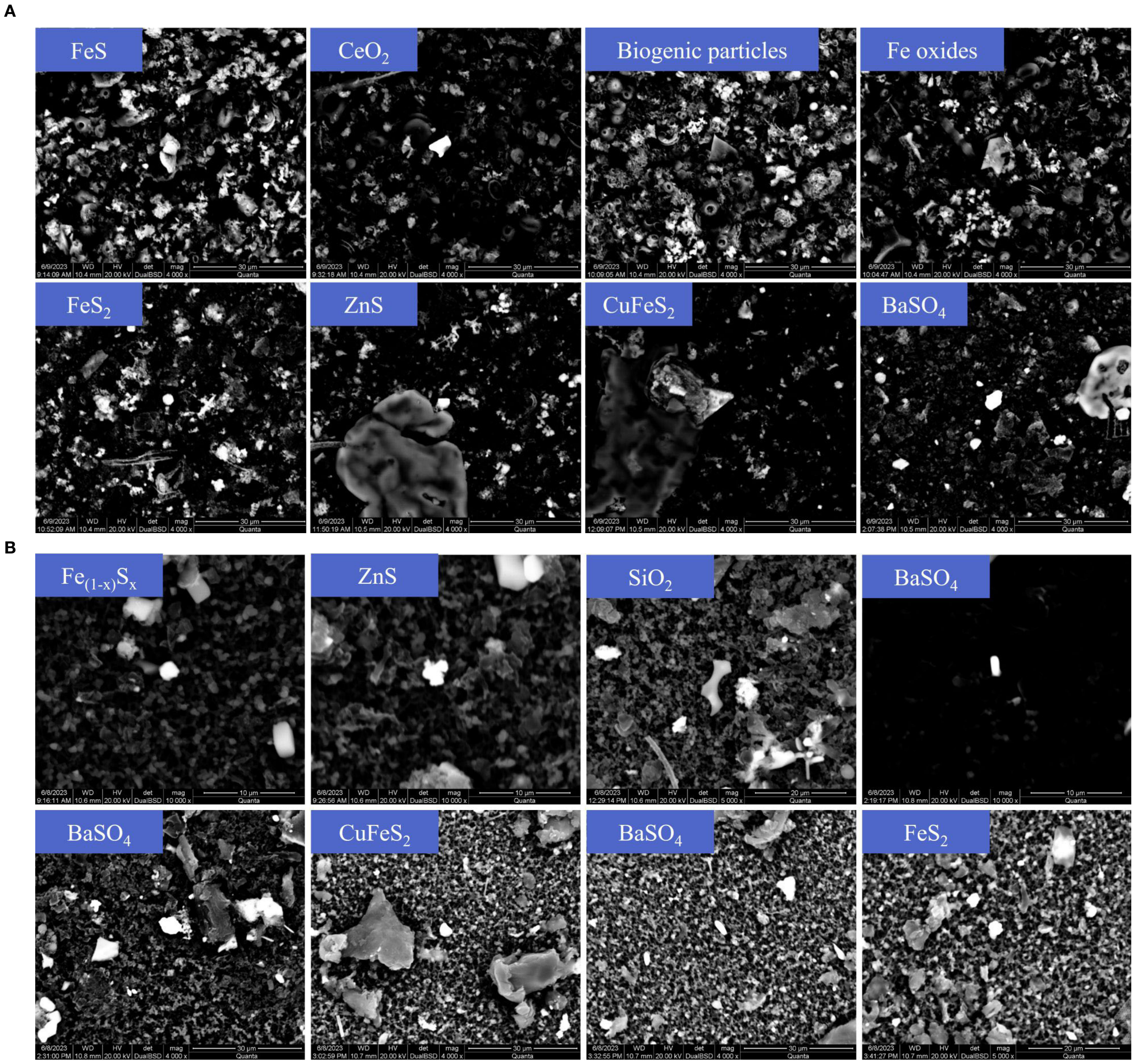

FIGURE 7
(A) SEM images of filter near the hydrothermal vent of Longqi. **(B)** SEM images of filter near the hydrothermal vent of Tiancheng.

information related to hydrothermal activities, offering valuable insights into complex hydrothermal systems (Dias and Barriga, 2006; Liao et al., 2018).

The measured major and minor element contents in selected sediment samples are reported in Table 4A. Visual observation on the selected surface sediment samples revealed that samples P1 to P9 are light gray, while P10 to P15 are reddish-brown, likely due to higher metal content from hydrothermal influence. The analytical results show that sediments P10–P15 have Fe contents ranging from 8.8% to 32.3%, with an average of 20.8%, significantly higher than those in sediments P1–P9 (0.4% – 3.2%, with an average of 1.21%). The Cu and Zn contents in sediments P10–P15 range from 182 µg/g to 130 mg/g (averaged to be 47 mg/g) and 74 µg/g to 33 mg/g (averaged to be 8.8 mg/g), respectively. These values are substantially higher than those in sediments P1–P9, where Cu and Zn contents range from 19 to 100 µg/g (averaged to be 52.8 µg/g) and 15 to 66 µg/g (averaged to be 40.6 µg/g), respectively.

The principal component analysis of the geochemistry data set was performed using IBM SPSS Statistics 25.0 software to further constrain the factors influencing the geochemistry data for the surface sediments in the study area (Supplementary Table S2). Three major factors with eigen values greater than 1 that together explain approximately 80% of the variance of the data set were extracted. And the PCA scores and loading Plot of surface sediment geochemistry is showed in Supplementary Figure S3. The dominant factor (Factor 1 (F1)) explains approximately 42% of the total

TABLE 4A Major and trace element concentrations of surface sediments.

Sample ID	Distance (km)	Fe %	Mn Mg/g	Cu µg/g	Zn µg/g	Al µg/g	Ti µg/g	Ca Mg/g	REY µg/g	$(Eu/Eu^*)_N$
P1	51.79	2.0	2.44	85	49	17	1073	261	156	0.72
P2	35.54	3.2	2.39	100	66	13	696	194	99	0.71
P3	418.71	1.2	0.72	69	72	9	601	320	79	0.67
P4	20.06	0.5	0.34	19	20	6	340	353	39	0.68
P5	658.94	0.7	0.56	35	25	8	515	330	66	0.70
P6	258.90	0.6	0.24	32	23	9	481	325	56	0.69
P7	655.96	1.8	1.52	64	56	20	1810	239	100	0.74
P8	558.30	0.4	0.29	25	15	4	278	347	46	0.70
P9	274.91	0.5	0.69	46	39	8	498	321	51	0.70
P10	1.03	18.5	0.80	130400	1277	2	41	6	17	1.10
P11	73.15	16.3	2.97	35260	33940	14	669	119	65	0.90
P12	166.58	32.3	0.01	58750	6878	1	5	2	7	3.39
P13	1.09	19.1	3.32	28860	4200	4	109	5	43	1.31
P14	0.08	8.8	3.21	182	74	76	4785	64	76	1.08
P15	0.37	29.8	24.8	29550	6609	2	181	4	16	2.18

TABLE 4B The Ba concentrations and Ba isotope compositions in surface sediments.

Sample ID	Type	Ba Concentrations (µg/g)	δ^{138}Ba ‰
P1	Background sediment	636	
P2	Background sediment	488	
P3	Background sediment	1109	0.14
P4	Background sediment	191	
P5	Background sediment	475	0.12
P6	Background sediment	548	
P7	Background sediment	1065	0.01
P8	Background sediment	350	
P9	Background sediment	645	
P10	Hydrothermal-impacted sediment	869	
P11	Hydrothermal-impacted sediment	413	-0.06
P12	Hydrothermal-impacted sediment	917	-0.14
P13	Hydrothermal-impacted sediment	273	0.01
P14	Hydrothermal-impacted sediment	248	-0.07
P15	Hydrothermal-impacted sediment	110	-0.16

variance and is loaded primarily with lithogenic elements, e.g., Fe, Cu, Pb, S, V, Zn, which frequently reflect the hydrothermal component. Factor 2 (F2), explaining a significant portion of the remaining variance, was predominantly associated with elevated Al and Ti concentrations, which are commonly used as lithogenic tracers. Factor 3 (F3) highlighted Ba enrichment, likely linked to marine authigenic processes, such as biogenic barite precipitation or scavenging by sinking organic matter. This tripartite structure

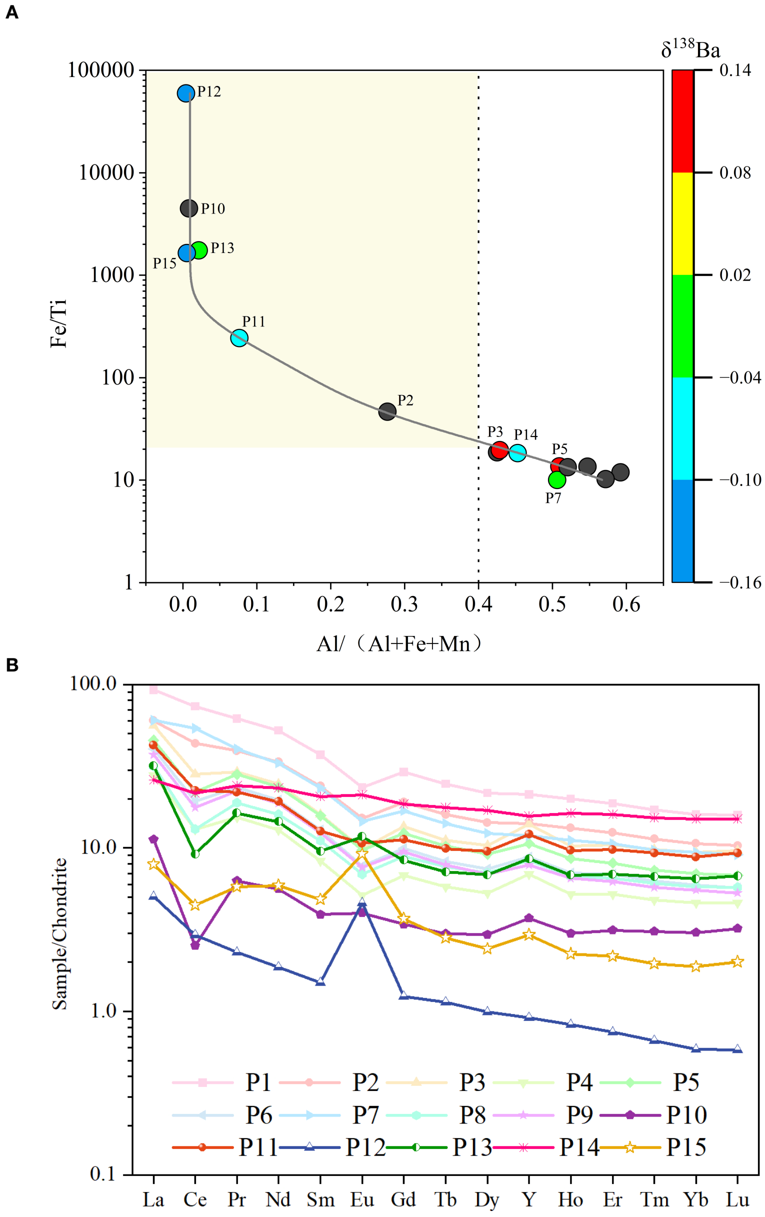

FIGURE 8
(A) Al/(Al+Fe+Mn) vs. Fe/Ti diagram (δ^{138}Ba as as X-axis color bar) of sediments. The black dots represents samples not analyzed for barium isotopes. **(B)** Chondrite-normalized REE distributions of the study area sediments. The chondrite data are from Boynton (1984).

underscores the interplay of hydrothermal activity, terrestrial sediment supply, and pelagic marine influences in shaping the geochemical signatures of the studied sediments.

The elemental ratios serve as a robust proxy for assessing hydrothermal input intensity (Qiu et al., 2023). To evaluate hydrothermal influence on sediments along the Southwest Indian Ridge, two geochemical indices were employed: (1) the metal enrichment index Al/(Al + Fe + Mn) and (2) the Fe/Ti ratio. These indices effectively differentiate hydrothermal contributions from detrital components in marine sediments.

The Al/(Al + Fe + Mn) index distinguishes metal-rich hydrothermal sediments from background sediments. Previous studies (e.g., Fisher et al., 1969; Dias and Barriga, 2006) established that background deep-sea sediments, devoid of hydrothermal input, typically exhibit values >40% due to higher detrital aluminosilicate content. In contrast, hydrothermal sediments near vent systems are characterized by lower values, reflecting Fe-Mn oxide dominance. Concurrently, the Fe/Ti ratio quantifies hydrothermal metal enrichment relative to detrital inputs, with ratios >20 indicating significant hydrothermal influence (Zhou et al., 2020). By cross-plotting these indices (Figure 8A), hydrothermal and detrital sediment sources can be systematically discriminated (Liao et al., 2018).

Application of this dual-index approach to 15 surface sediment samples revealed distinct geochemical signatures. Six samples (P2, P10–P13, P15) exhibited Fe/Ti >20 coupled with Al/(Al + Fe + Mn) <40%, unambiguously identifying them as hydrothermal-impacted sediments (Figure 8A). These results align with established thresholds and underscore the utility of combining elemental ratios to disentangle complex sedimentary provenance.

Another way to identify the significance of hydrothermal activity on surface sediments is by looking into the rare earth element (REE) composition in sediments. The hydrothermal fluids from mid-ocean ridges are characterized by Light REE (LREE) enrichment and positive Eu anomalies (Douville et al., 1999; Allen and Seyfried, 2005; Cao et al., 2012). Consequently, sediments affected by hydrothermal activity often exhibit similar characteristics (Gillis and Thompson, 1993; Liao et al., 2018; Zhou et al., 2020). The Chondrite-normalized REE patterns of the sediment samples are shown in Figure 8B. In general, all sediment samples showed a trend of LREE enrichment. Whilst, several samples (from P10 to P15), to different extents, showed apparent positive Eu anomaly ($(Eu/Eu^*)_N = 0.90–3.39$) compared to the value (0.71) reported by Liao et al. (2018) for the background sediments.

It is specifically noted that although the metal ratios of P14 exceed the predicted range, they fall near the threshold boundaries. Additionally, P14 exhibits elevated Fe, Cu, and Zn concentrations compared to samples P1–P9, while its Ca content is significantly lower. Visually, the sample displays a reddish-brown coloration—a characteristic indicative of hydrothermal activity. Based on this integrated evidence, we have classified P14 as hydrothermal-impacted sediment. The sediment types are explicitly detailed in Table 4B. Overall, by taking into consideration of the results, we considered that, among the 15 surface sediment samples, P10 to P15 can be identified as hydrothermal-impacted sediments, and that P1 to P9 represent background sediments.

3.3.2 Ba contents and Ba isotope compositions

Following sediment classification, we measured the Ba contents across all samples and selected eight representative samples for Ba isotope analysis. This subset included three background sediments (P3, P5, P7) and five hydrothermal sediments (P11 to P15). The Ba contents and its isotopic compositions in sediment samples are reported in Table 4B. The Ba content ranged from 110–1109 μg/g, and there is no apparent elevation in Ba content in hydrothermal influenced samples. Paytan and Griffith (2007) reported that the content of Ba in marine sediments can be significantly affected by dilution effects due to the accumulation of other sedimentary components.

To the contrary, the δ^{138}Ba values in background samples (P3, P5,P7) ranged from 0.01‰ to 0.14‰, similar to the deep-sea sediments reported in previous study (0 – 0.10‰) (Bridgestock et al., 2018). In hydrothermal-impacted sediments (P11 to P15), δ^{138}Ba values ranged from -0.16‰ – 0.01‰. The average δ^{138}Ba of hydrothermal sediments (-0.08‰, SD=0.07‰, *n=5*) is notably lower than that of the background sediments (0.09‰, SD=0.07‰, *n=3*). The relationship of Ba contents and δ^{138}Ba is shown in Supplementary Figure S4. The results show that the data points do not follow a distinct fractionation trend (i.e., lighter Ba isotopes correlating with higher Ba concentrations). Instead, samples with lighter Ba isotopes exhibit both high and low Ba concentrations. We therefore propose that the Ba concentrations in hydrothermal-impacted sediments are influenced by dilution effects from co-occurring hydrothermal metal elements.

As we discussed in section 3.2.3, during the mixing process between hydrothermal fluid and seawater, lighter Ba isotopes are preferentially removed, resulting the settling particles compose lighter Ba isotope. This is consistent with our observation in the hydrothermally influenced sediment samples in this study. As conclusion, while the Ba content of hydrothermal sediments cannot be distinguished from the background sediments, the Ba isotope retains lighter isotopic signature, potentially can serve as an indicator of hydrothermal influence on sediment of the study region.

4 Conclusion

Although the overall Ba cycle in the ocean is relatively well understood, studies focusing on specific processes, such as hydrothermal activities, remain limited. This study presents the first Ba isotope study in hydrothermal fluid, seawater, and sediment near Southwest Indian Ocean hydrothermal vent field.

The vertical profiles of dissolved Ba and its isotope compositions is similar with previous results of other oceans. The $[Ba]_{diss}$ in several water samples collected using ROV near hydrothermal vents are significantly higher than background seawater, while the Ba isotope compositions in those samples (-0.10 – 0.05‰) are distinctly lower than those of background seawater(~ 0.29‰), suggesting that the hydrothermal fluids in the study region bearing lighter Ba isotopes.

Analysis of filter membranes from Longqi and Tiancheng hydrothermal vents samples using Scanning Electron Microscopy and Energy-Dispersive X-ray Spectroscopy revealed that, various mineral species exist, not only barite, but also Fe oxides, FeS, FeS_2, $Fe_{(1-x)}$ Sx, CeO_2, ZnS, and SiO_2, etc. Therefore, barium may co-precipitate with iron-manganese oxides and metal sulfide particles in addition to forming barite, which processes could result in different isotopic fractionation.

Analysis of hydrothermally influenced sediment showed that the Ba isotope compositions are significantly lighter (-0.16‰ – 0.01‰) compared to those in background sediments (0.01 – 0.14‰), which is consistent with lighter isotope composition found in hydrothermal fluid and also align with the calculation result of the Rayleigh fractionation model, suggesting lighter isotopes are preferable removed during the mixing process between hydrothermal fluid and seawater. Therefore, the Ba isotope may serve as a valuable indicator of hydrothermal influence in future studies on sediment.

Data availability statement

The original contributions presented in the study are included in the article/Supplementary Material. Further inquiries can be directed to the corresponding authors.

Author contributions

CZ: Formal Analysis, Investigation, Visualization, Writing – original draft. LL: Conceptualization, Data curation, Project administration, Supervision, Validation, Writing – original draft, Writing – review & editing. JL: Data curation, Investigation, Methodology, Writing – original draft. RX: Conceptualization, Data curation, Formal Analysis, Writing – review & editing. XW: Data curation, Investigation, Methodology, Writing – original draft. XS: Funding acquisition, Project administration, Resources, Writing – review & editing.

Funding

The author(s) declare that financial support was received for the research and/or publication of this article. Natural Science Foundation of China (42076046,42376035)National Key Research and Development Program of China (2022YEE0136055).

Acknowledgments

The authors would like to thank the captain and crew of the *R/V Da Yang 1* and *R/V Dayang* and the pilots of the ROV *Hailong III* for their skilled operations and technical support at sea. We want to thank all the colleagues and students who have helped at sea or in the laboratory to make this work possible. This work was supported by the Natural Science Foundation of China (42076046, 42376035), the National Key Research and Development Program of China (2022YFE0136500).

Conflict of interest

The authors declare that the research was conducted in the absence of any commercial or financial relationships that could be construed as a potential conflict of interest.

Generative AI statement

The author(s) declare that no Generative AI was used in the creation of this manuscript.

Publisher's note

Supplementary material

The Supplementary Material for this article can be found online at: https://www.frontiersin.org/articles/10.3389/fmars.2025.1538835/full#supplementary-material

References

Agarwal, D. K., Roy, P., Prakash, L. S., and Kurian, P. J. (2020). Hydrothermal signatures in sediments from eastern Southwest Indian Ridge 63°E to 68°E. *Mar. Chem.* 218, 103732. doi: 10.1016/j.marchem.2019.103732

Allen, D. E., and Seyfried, W. E. (2005). REE controls in ultramafic hosted MOR hydrothermal systems: An experimental study at elevated temperature and pressure. *Geochimica Cosmochimica Acta* 69, 675–683. doi: 10.1016/j.gca.2004.07.016

Alt, J. C. (1995). Subseafloor processes in mid-ocean ridge hydrothermal systems. *Seafloor Hydrothermal Systems: Physical Chemical Biological Geological Interact.* 91. doi: 10.1029/GM091p0085

Bates, S. L., Hendry, K. R., Pryer, H. V., Kinsley, C. W., Pyle, K. M., Woodward, E. M. S., et al. (2017). Barium isotopes reveal role of ocean circulation on barium cycling in the Atlantic. *Geochimica Cosmochimica Acta* 204, 286–299. doi: 10.1016/j.gca.2017.01.043

Bennett, S. A., Rouxel, O., Schmidt, K., Garbe-Schönberg, D., Statham, P. J., and German, C. R. (2009). Iron isotope fractionation in a buoyant hydrothermal plume, 5 S Mid-Atlantic Ridge. *Geochimica Cosmochimica Acta* 73, 5619–5634. doi: 10.1016/j.gca.2009.06.027

Boynton, W. V. (1984). Cosmochemistry of the rare earth elements: meteorite studies[J]. *Dev. Geochem.* 2, 63–114. doi: 10.1016/B978-0-444-42148-7.50008-3

Bridgestock, L., Hsieh, Y.-T., Porcelli, D., Homoky, W. B., Bryan, A., and Henderson, G. M. (2018). Controls on the barium isotope compositions of marine sediments. *Earth Planetary Sci. Lett.* 481, 101–110. doi: 10.1016/j.epsl.2017.10.019

Bridgestock, L., Nathan, J., Paver, R., Hsieh, Y.-T., Porcelli, D., Tanzil, J., et al. (2021). Estuarine processes modify the isotope composition of dissolved riverine barium fluxes to the ocean. *Chem. Geology* 579, 120340. doi: 10.1016/j.chemgeo.2021.120340

Butterfield, D. A., and Massoth, G. J. (1994). Geochemistry of north Cleft segment vent fluids: Temporal changes in chlorinity and their possible relation to recent volcanism. *J. Geophysical Research: Solid Earth* 99, 4951–4968. doi: 10.1029/93jb02798

Cannat, M., Sauter, D., Bezos, A., Meyzen, C., Humler, E., and Le Rigoleur, M. (2008). Spreading rate, spreading obliquity, and melt supply at the ultraslow spreading Southwest Indian Ridge. *Geochemistry Geophysics Geosystems* 9 (4). doi: 10.1029/2007gc001676

Cao, Z., Cao, H., Tao, C., Li, J., Yu, Z., and Shu, L. (2012). Rare earth element geochemistry of hydrothermal deposits from Southwest Indian Ridge. *Acta Oceanologica Sin.* 31, 62–69. doi: 10.1007/s13131-012-0192-1

Cao, Z., Li, Y., Rao, X., Yu, Y., Hathorne, E. C., Siebert, C., et al. (2020). Constraining barium isotope fractionation in the upper water column of the South China Sea. *Geochimica Cosmochimica Acta* 288, 120–137. doi: 10.1016/j.gca.2020.08.008

Cao, Z., Rao, X., Yu, Y., Siebert, C., Hathorne, E. C., Liu, B., et al. (2021). Stable barium isotope dynamics during estuarine mixing. *Geophysical Res. Lett.* 48 (19). doi: 10.1029/2021gl095680

Cao, Z., Siebert, C., Hathorne, E. C., Dai, M., and Frank, M. (2016). Constraining the oceanic barium cycle with stable barium isotopes. *Earth Planetary Sci. Lett.* 434, 1–9. doi: 10.1016/j.epsl.2015.11.017

Carter, S. C., Paytan, A., and Griffith, E. M. (2020). Toward an improved understanding of the marine barium cycle and the application of marine barite as a paleoproductivity proxy. *Minerals* 10, 421. doi: 10.3390/min10050421

Chen, J., Tao, C. H., Liang, J., Liao, S. L., Dong, C. W., Li, H. M., et al. (2018). Newly discovered hydrothermal fields along the ultraslow-spreading Southwest Indian Ridge around 63°E. *Acta Oceanologica Sin.* 37, 61–67. doi: 10.1007/s13131-018-1333-y

Coogan, L. A., Seyfried, W. E., and Pester, N. J. (2019). Environmental controls on mid-ocean ridge hydrothermal fluxes. *Chem. Geology* 528, 119285. doi: 10.1016/j.chemgeo.2019.119285

Crockford, P. W., Wing, B. A., Paytan, A., Hodgskiss, M. S. W., Mayfield, K. K., Hayles, J. A., et al. (2019). Barium-isotopic constraints on the origin of post-Marinoan barits. *Earth Planetary Sci. Lett.* 519, 234–244. doi: 10.1016/j.epsl.2019.05.018

Demets, C., Gordon, R. G., Argus, D. F., and Stein, S. (1994). Effect of recent revisions to the geomagnetic reversal time scale on estimates of current plate motions. *John Wiley Sons Ltd.* 21, 2091–2094. doi: 10.1029/94GL02118

Dias, A. S., and Barriga, F. J. (2006). Mineralogy and geochemistry of hydrothermal sediments from the serpentinite-hosted Saldanha hydrothermal field (36 34′ N; 33 26′ W) at MAR. *Mar. Geology* 225, 157–175. doi: 10.1016/j.margeo.2005.07.013

Douville, E., Bienvenu, P., Charlou, J. L., Donval, J. P., Fouquet, Y., Appriou, P., et al. (1999). Yttrium and rare earth elements in fluids from various deep-sea hydrothermal systems. *Geochimica Cosmochimica Acta* 63, 627–643. doi: 10.1016/S0016-7037(99)00024-1

Dymond, J., Suess, E., and Lyle, M. (1992). Barium in deep-sea sediment: A geochemical proxy for paleoproductivity. *PALEOCEANOGRAPHY.* 7, 163–181. doi: 10.1029/92PA00181

Eagle, M., Paytan, A., Arrigo, K. R., van Dijken, G., and Murray, R. W. (2003). A comparison between excess barium and barite as indicators of carbon export. *Paleoceanography* 18 (1). doi: 10.1029/2002pa000793

Elderfield, H., and Schultz, A. (1996). Mid-ocean ridge hydrothermal fluxes and the chemical composition of the ocean. *Annu. Rev. Earth Planetary Sci.* 24, 191–224. doi: 10.1146/annurev.earth.24.1.191

Fang, Z., and Wang, W.-X. (2021). Size speciation of dissolved trace metals in hydrothermal plumes on the Southwest Indian Ridge. *Sci. Total Environ.* 771, 145367. doi: 10.1016/j.scitotenv.2021.145367

Feely, R. A., Lewison, M., Massoth, G. J., Robert-Baldo, G., Lavelle, J. W., Byrne, R. H., et al. (1987). Composition and dissolution of black smoker particulates from active vents on the Juan de Fuca Ridge. *J. Geophysical Research: Solid Earth* 92, 11347–11363. doi: 10.1029/JB092iB11p11347

Findlay, A. J., Estes, E. R., Gartman, A., Yücel, M., Kamyshny, A. Jr., and Luther, III, G. W. (2019). Iron and sulfide nanoparticle formation and transport in nascent hydrothermal vent plumes. *Nat. Commun.* 10, 1597. doi: 10.1038/s41467-019-09580-5

Fisher, D. E., Joensuu, O., and Boström, K. (1969). Elemental abundances in ultramafic rock and their relation to the upper mantle. *J. Geophysical Res.* 74, 3865–3873. doi: 10.1029/JB074i015p03865

Fitzsimmons, J. N., John, S. G., Marsay, C. M., Hoffman, C. L., Nicholas, S. L., Toner, B. M., et al. (2017). Iron persistence in a distal hydrothermal plume supported by dissolved–particulate exchange. *Nat. Geosci.* 10, 195–201. doi: 10.1038/ngeo2900

Fu, W. W., and Wang, W. L. (2022). Biogeochemical equilibrium responses to maximal productivity in high nutrient low chlorophyll regions. *J. Geophysical Research-Biogeosciences* 127 (5). doi: 10.1029/2021jg006636

Gallant, R. M., and Von Damm, K. L. (2006). Geochemical controls on hydrothermal fluids from the Kairei and Edmond Vent Fields, 23°-25°S. *Cent. Indian Ridge Geochemistry Geophysics Geosystems* 7 (6). doi: 10.1029/2005gc001067

Gartman, A., Findlay, A. J., Hannington, M., Garbe-Schönberg, D., Jamieson, J. W., and Kwasnitschka, T. (2019). The role of nanoparticles in mediating element deposition and transport at hydrothermal vents. *Geochimica Cosmochimica Acta* 261, 113–131. doi: 10.1016/j.gca.2019.06.045

Gillis, K. M., and Thompson, G. (1993). Metabasalts from the Mid-Atlantic Ridge: new insights into hydrothermal systems in slow-spreading crust. *Contributions to Mineralogy Petrology* 113, 502–523. doi: 10.1007/BF00698319

Hawkes, J. A., Connelly, D., Gledhill, M., and Achterberg, E. P. (2013). The stabilisation and transportation of dissolved iron from high temperature hydrothermal vent systems. *Earth Planetary Sci. Lett.* 375, 280–290. doi: 10.1016/j.epsl.2013.05.047

Horner, T. J., and Crockford, P. W. (2021). Barium Isotopes, geochemical tracers in earth system science. doi: 10.1017/9781108865845

Horner, T. J., Kinsley, C. W., and Nielsen, S. G. (2015). Barium-isotopic fractionation in seawater mediated by barite cycling and oceanic circulation. *Earth Planetary Sci. Lett.* 430, 511–522. doi: 10.1016/j.epsl.2015.07.027

Hsieh, Y.-T., Bridgestock, L., Scheuermann, P. P., Seyfried, W. E., and Henderson, G. M. (2021). Barium isotopes in mid-ocean ridge hydrothermal vent fluids: A source of isotopically heavy Ba to the ocean. *Geochimica Cosmochimica Acta* 292, 348–363. doi: 10.1016/j.gca.2020.09.037

Hsieh, Y.-T., and Henderson, G. M. (2017). Barium stable isotopes in the global ocean: Tracer of Ba inputs and utilization. *Earth Planetary Sci. Lett.* 473, 269–278. doi: 10.1016/j.epsl.2017.06.024

Jacquet, S. H. M., Dehairs, F., Cardinal, D., Navez, J., and Delille, B. (2005). Barium distribution across the Southern Ocean frontal system in the Crozet–Kerguelen Basin. *Mar. Chem.* 95, 149–162. doi: 10.1016/j.marchem.2004.09.002

Jamieson, J. W., Hannington, M. D., Tivey, M. K., Hansteen, T., Williamson, N. M. B., Stewart, M., et al. (2016). Precipitation and growth of barite within hydrothermal vent deposits from the Endeavour Segment, Juan de Fuca Ridge. *Geochimica Cosmochimica Acta* 173, 64–85. doi: 10.1016/j.gca.2015.10.021

Ji, F., Zhou, H., Yang, Q., Gao, H., Wang, H., and Lilley, M. D. (2017). Geochemistry of hydrothermal vent fluids and its implications for subsurface processes at the active Longqi hydrothermal field, Southwest Indian Ridge. *Deep Sea Res. Part I: Oceanographic Res. Papers* 122, 41–47. doi: 10.1016/j.dsr.2017.02.001

Kumagai, H., Nakamura, K., Toki, T., Morishita, T., Okino, K., Ishibashi, J., et al. (2008). Geological background of the Kairei and Edmond hydrothermal fields along the Central Indian Ridge: Implications of their vent fluids' distinct chemistry. *Geofluids* 8, 239–251. doi: 10.1111/j.1468-8123.2008.00223.x

Lea, D. W. (1993). CONSTRAINTS ON THE ALKALINITY AND CIRCULATION OF GLACIAL CIRCUMPOLAR DEEP-WATER FROM BENTHIC FORAMINIFERAL BARIUM. *Global Biogeochemical Cycles* 7, 695–710. doi: 10.1029/93gb01536

Lea, D., and Boyle, E. (1989). Barium content of benthic foraminifera controlled by bottom-water composition. *Nature* 338, 751–753. doi: 10.1038/338751a0

Lea, D. W., and Boyle, E. A. (1991). BARIUM IN PLANKTONIC-FORAMINIFERA. *Geochimica Et Cosmochimica Acta* 55, 3321–3331. doi: 10.1016/0016-7037(91)90491-m

Li, L., Liu, J., Wang, X., and Shi, X. (2015). Dissolved trace metal distributions and Cu speciation in the southern Bohai Sea. *China Mar. Chem.* 172, 34–45. doi: 10.1016/j.marchem.2015.03.002

Li, M., Toner, B. M., Baker, B. J., Breier, J. A., Sheik, C. S., and Dick, G. J. (2014). Microbial iron uptake as a mechanism for dispersing iron from deep-sea hydrothermal vents. *Nat. Commun.* 5, 3792. doi: 10.1038/ncomms4192

Liao, S., Tao, C., Li, H., Zhang, G., Liang, J., Yang, W., et al. (2018). Surface sediment geochemistry and hydrothermal activity indicators in the Dragon Horn area on the Southwest Indian Ridge. *Mar. Geology* 398, 22–34. doi: 10.1016/j.margeo.2017.12.005

Lin, Y.-B., Wei, H.-Z., Jiang, S.-Y., Hohl, S., Lei, H.-L., Liu, X., et al. (2020). Accurate determination of barium isotopic compositions in sequentially leached phases from carbonates by double spike-Thermal ionization mass spectrometry (DS-TIMS). *Analytical Chem.* 92, 2417–2424. doi: 10.1021/acs.analchem.9b03137

Lin, Y.-B., Wei, H.-Z., Zhang, F., Hohl, S. V., Wei, G.-Y., Li, T., et al. (2022). Evaluation of shallow-water corals and associated carbonate sediments as seawater Ba isotope archives in the South China Sea. *Palaeogeography Palaeoclimatology Palaeoecol.* 605. doi: 10.1016/j.palaeo.2022.111196

Lough, A., Homoky, W., Connelly, D., Comer-Warner, S., Nakamura, K., Abyaneh, M., et al. (2019). Soluble iron conservation and colloidal iron dynamics in a hydrothermal plume. *Chem. Geology* 511, 225–237. doi: 10.1016/j.chemgeo.2019.01.001

McCulloch, M., Fallon, S., Wyndham, T., Hendy, E., Lough, J., and Barnes, D. (2003). Coral record of increased sediment flux to the inner Great Barrier Reef since European settlement. *Nature* 421, 727–730. doi: 10.1038/nature01361

McManus, J., Berelson, W. M., Hammond, D. E., and Klinkhammer, G. P. (1999). Barium cycling in the north pacific: implications for the utility of ba as a paleoproductivity and paleoalkalinity proxy. *Paleoceanography* 14, 53–61. doi: 10.1029/1998pa900007

Middleton, J. T., Hong, W. L., Paytan, A., Auro, M. E., Griffith, E. M., and Horner, T. J. (2023). Barium isotope fractionation in barite–fluid systems at chemical equilibrium. *Chem. Geology* 627, 121453. doi: 10.1016/j.chemgeo.2023.121453

Mori, C., Santos, I. R., Brumsack, H.-J., Schnetger, B., Dittmar, T., and Seidel, M. (2019). Non-conservative behavior of dissolved organic matter and trace metals (Mn, Fe, Ba) driven by porewater exchange in a subtropical mangrove-estuary. *Front. Mar. Sci.* 6. doi: 10.3389/fmars.2019.00481

Mottl, M. J., Holland, H. D., and Corr, R. F. (1978). Chemical exchange during hydrothermal alteration of basalt by seawater—II. Experimental results for Fe, Mn, and sulfur species. *Geochimica Et Cosmochimica Acta* 43, 869–884. doi: 10.1016/0016-7037(79)90225-4

Nielsen, S. G., Horner, T. J., Pryer, H. V., Blusztajn, J., Shu, Y., Kurz, M. D., et al. (2018). Barium isotope evidence for pervasive sediment recycling in the upper mantle. *Sci. Adv.* 4, sciadv.aas8675. doi: 10.1126/sciadv.aas8675

Nishioka, J., Obata, H., and Tsumune, D. (2013). Evidence of an extensive spread of hydrothermal dissolved iron in the Indian Ocean. *Earth Planetary Sci. Lett.* 361, 26–33. doi: 10.1016/j.epsl.2012.11.040

Paytan, A., and Griffith, E. M. (2007). : Marine barite: Recorder of variations in ocean export productivity. *Deep Sea Res. Part II: Topical Stud. Oceanography* 54, 687–705. doi: 10.1016/j.dsr2.2007.01.007

Paytan, A., and Kastner, M. (1996). Benthic Ba fluxes in the central Equatorial Pacific, implications for the oceanic Ba cycle. *Earth Planetary Sci. Lett.* 142, 439–450. doi: 10.1016/0012-821X(96)00120-3

Pretet, C. (2013). *Non-traditional isotopes (Barium and Calcium) and elemental ratios in scleractinian coral skeleton: new look into geochemical cycles, environmental proxies and bio-calcification processes* (Switzerland: Section des sciences de la Terre et de l'environnement, Université de Genève). doi: 10.13097/archive-ouverte/unige:33163

Qiu, Z., Han, X., Fan, W., Wang, Y., Li, M., and Cai, Y. (2023). Hydrothermal signatures and prospecting indicators in sediments along the Carlsberg Ridge. *Sedimentary Geology* 458, 106536. doi: 10.1016/j.sedgeo.2023.106536

Resing, J. A., Sedwick, P. N., German, C. R., Jenkins, W. J., Moffett, J. W., Sohst, B. M., et al. (2015). Basin-scale transport of hydrothermal dissolved metals across the South Pacific Ocean. *Nature* 523, 200–U140. doi: 10.1038/nature14577

Rippert, N., Baumann, K.-H., and PÄTzold, J. (2015). Thermocline fluctuations in the western tropical Indian Ocean during the past 35 ka. *J. Quaternary Sci.* 30, 201–210. doi: 10.1002/jqs.2767

Roeske, T., Rutgers vd Loeff, M., Middag, R., and Bakker, K. (2012). Deep water circula-tion and composition in the Arctic Ocean by dissolved barium, aluminium and silicate. *Mar. Chem.* 132–133, 56–67. doi: 10.1016/j.marchem.2012.02.001

Rouxel, O., Shanks, W. C. III, Bach, W., and Edwards, K. J. (2008). Integrated Fe-and S-isotope study of seafloor hydrothermal vents at East Pacific Rise 9–10 N, Chemical Geology. *Chemical Geology* 252, 214–227. doi: 10.1016/j.chemgeo.2008.03.009

Rouxel, O., Toner, B. M., Manganini, S. J., and German, C. R. (2016). Geochemistry and iron isotope systematics of hydrothermal plume fall-out at East Pacific Rise 9°50′N. *Chem. Geology* 441, 212–234. doi: 10.1016/j.chemgeo.2016.08.027

Schlitzer, R., Anderson, R. F., Dodas, E. M., Lohan, M., Geibert, W., Tagliabue, A., et al. (2018). The GEOTRACES intermediate data product 2017. *Chem. Geology* 493, 210–223. doi: 10.1016/j.chemgeo.2018.05.040

Seyfried, W. E., Pester, N. J., Ding, K., and Rough, M. (2011). Vent fluid chemistry of the Rainbow hydrothermal system (36°N, MAR): Phase equilibria and in *situ* pH controls on subseafloor alteration processes. *Geochimica Cosmochimica Acta* 75, 1574–1593. doi: 10.1016/j.gca.2011.01.001

Tao, C., Lin, J., Guo, S., Chen, Y. J., Wu, G., Han, X., et al. (2012). First active hydrothermal vents on an ultraslow-spreading center: Southwest Indian Ridge. *Geology* 40, 47–50. doi: 10.1130/g32389.1

Tao, C., Xiong, W., Xi, Z., Deng, X., and Xu, Y. (2014). TEM investigations of South Atlantic Ridge 13.2°S hydrothermal area. *Acta Oceanologica Sin.* 32, 68–74. doi: 10.1007/s13131-013-0392-3

Von Damm, ,. K. L. (1985). Chemistry of submarine hydrothermal solutions at 21°N, East Pacific Rise. *Geochimica Et Cosmochimica Acta* 49, 2197–2220. doi: 10.1016/0016-7037(85)90222-4

Whitmore, L. M., Shiller, A. M., Horner, T. J., Xiang, Y., Auro, M. E., Bauch, D., et al. (2022). Strong margin influence on the arctic ocean barium cycle revealed by pan-arctic synthesis. *J. geophysical Res. Oceans* 127, e2021JC017417. doi: 10.1029/2021JC017417

Yu, Y., Xie, R. C., Gutjahr, M., Laukert, G., Cao, Z., Hathorne, E., et al. (2022). High latitude controls on dissolved barium isotope distributions in the global ocean. *Geochemical Perspect. Lett.* 24, 22–26. doi: 10.7185/geochemlet.2242

Yuan, B., Yang, Y. M., Yu, H. J., Zhao, Y. X., Ding, Q. F., Yang, J. C., et al. (2018). Geochemistry of pyrite and chalcopyrite from an active black smoker in 49.6A°E Southwest Indian Ridge. *Mar. Geophysical Res.* 39, 441–461. doi: 10.1007/s11001-017-9324-5

Zhang, H., Luo, Y., Yu, J., Zhang, L., Xiang, R., Yu, Z., et al. (2022). Indian Ocean sedimentary calcium carbonate distribution and its implications for the glacial deep ocean circulation. *Quaternary Sci. Rev.* 284, 107490. doi: 10.1016/j.quascirev.2022.107490

Zhang, Z., Zhou, L., Chen, X.-G., Achterberg, E. P., Yu, Y., Hathorne, E., et al. (2024). Introduction of isotopically light barium from the Rainbow hydrothermal system into the deep Atlantic Ocean. *Earth Planetary Sci. Lett.* 625, 118476. doi: 10.1016/j.epsl.2023.118476

Zhou, T., Shi, X., Huang, M., Yu, M., Bi, D., Ren, X., et al. (2020). The influence of hydrothermal fluids on the REY-rich deep-sea sediments in the yupanqui basin, eastern south pacific ocean: constraints from bulk sediment geochemistry and mineralogical characteristics. *Minerals* 10, 1141. doi: 10.3390/min10121141